ACS PHYSICAL CHEMISTRY Au
AN OPEN ACCESS JOURNAL OF THE AMERICAN CHEMICAL SOCIETY

pubs.acs.org/physchemau
Article

Raman Spectroscopic Insights of Phase-Separated Insulin Aggregates

Published as part of ACS Physical Chemistry Au virtual special issue "Ultrafast Spectroscopy of Chemical Transformations".

Sandip Dolui, Anupam Roy, Uttam Pal, Shubham Kundu, Esha Pandit, Bhisma N Ratha, Ranit Pariary, Achintya Saha, Anirban Bhunia, and Nakul C. Maiti*

Cite This: ACS Phys. Chem Au 2024, 4, 268–280
Read Online

ABSTRACT: Phase-separated protein accumulation through the formation of several aggregate species is linked to the pathology of several human disorders and diseases. Our current investigation envisaged detailed Raman signature and structural intricacy of bovine insulin in its various forms of aggregates produced in situ at an elevated temperature (60 °C). The amide I band in the Raman spectrum of the protein in its native-like conformation appeared at 1655 cm^{-1} and indicated the presence of a high content of α-helical structure as prepared freshly in acidic pH. The disorder content (turn and coils) also was predominately present in both the monomeric and oligomeric states and was confirmed by the presence shoulder amide I maker band at ∼1680 cm^{-1}. However, the band shifted to ∼1671 cm^{-1} upon the transformation of the protein solution into fibrillar aggregates as produced for a longer time of incubation. The protein, however, maintained most of its helical conformation in the oligomeric phase; the low-frequency backbone α-helical conformation signal at ∼935 cm^{-1} was similar to that of freshly prepared aqueous protein solution enriched in helical conformation. The peak intensity was significantly weak in the fibrillar aggregates, and it appeared as a good Raman signature to follow the phase separation and the aggregation behavior of insulin and similar other proteins. Tyrosine phenoxy moieties in the protein may maintained its H-bond donor−acceptor integrity throughout the course of fibril formation; however, it entered in more hydrophobic environment in its journey of fibril formation. In addition, it was noticed that oligomeric bovine insulin maintained the orientation/conformation of the disulfide bonds. However, in the fibrillar state, the disulfide linkages became more strained and preferred to maintain a single conformation state.

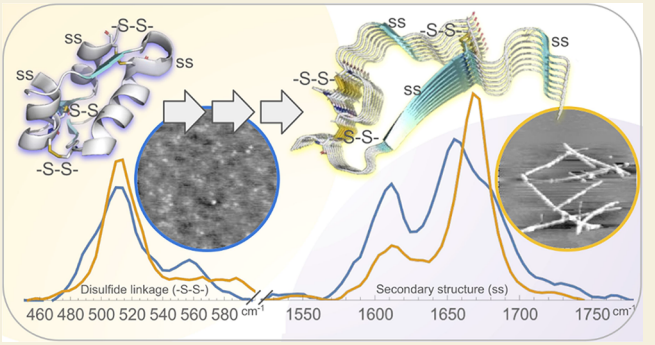

KEYWORDS: *amyloid, tyrosine, fermi doublet, fluorescence, aggregation, phase separation*

INTRODUCTION

Protein misfolding and fibrillization of well-defined globular proteins and intrinsically disordered proteins (IDPs) have emerged as an important pathological signature and a key molecular marker of various amyloid-related human diseases and disorders.[1−13] While IDPs remained energetically at higher energy state, a high rate of thermal fluctuation rendered its stability entropically favorable. However, hydrophobic interactions and subsequent zipping among amyloidogenic regions of disordered proteins lead to the formation of water-insoluble and thermodynamically more stable β-sheet-rich protein fibrils.[14,15] Thus, protein kinematics plays a significant role in the stability of disordered proteins in the solution phase. However, highly folded globular proteins in their native states are quite stable mainly due to their folded structure stabilized by different noncovalent molecular interactions.[16,17] Disulfide linkages also, in some cases, added additional stability to their tertiary folded structure.[18] Thus, the folded proteins are much in a lower energy state compared to IDPs. Therefore, heat or other harsh conditions (low pH, addition of salt, denaturants) are often required for globular protein to unfold fully or partially to initiate the aggregation and fibrilization process.[19−23]

It has been well established through several in situ investigations that the fibril formation of both types of proteins, IDPs and globular, proceeds via formation of soluble oligomeric state, regardless of the initial incubation conditions

Received: November 30, 2023
Revised: January 30, 2024
Accepted: January 31, 2024
Published: February 15, 2024

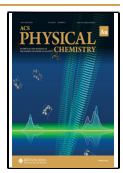

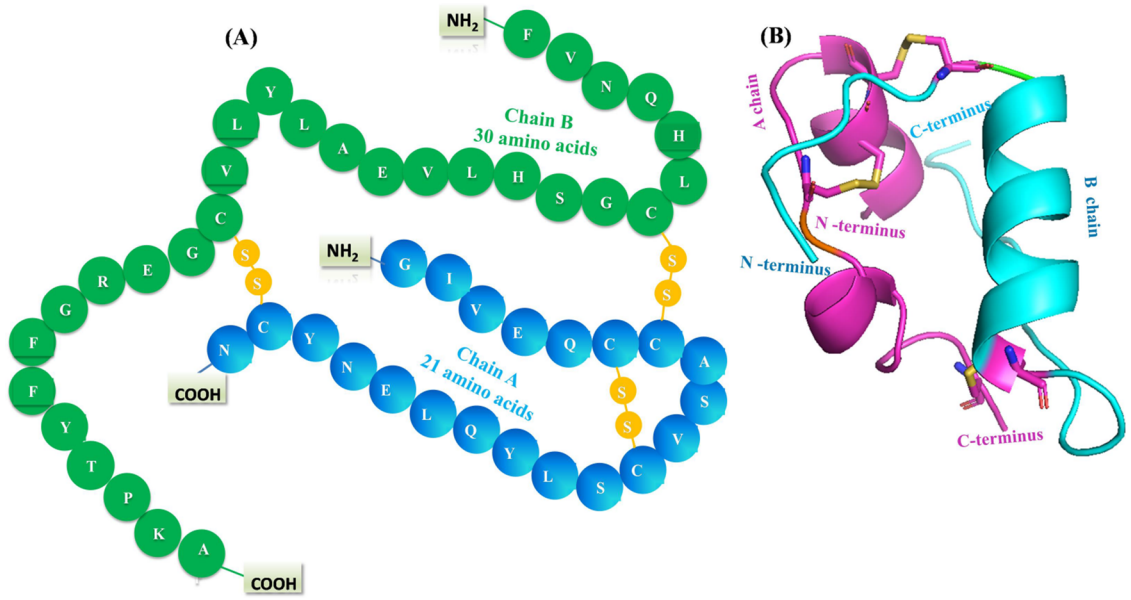

Figure 1. (A) Primary amino acid sequences with typical intra- and interchain disulfide bonding (interconnecting yellow lines) of BI. Twenty amino acids make up the A-chain (blue), whereas 30 amino acids make up the B-chain (green). These chains are connected by two intrachain and one interchain disulfide bridges. The secondary structure of insulin is shown in the right panel (RCSB PDB) entry 2ZP6; illustrated in Pymol). There are two α-helices in the A-chain (pink). The cyan B-chain has a random coil in addition to an α helix.

of the protein solution.[24,25] These oligomeric intermediates are not always water-insoluble; however, they may be considered as a separate liquid phase entity and are significantly different from a clear monomeric protein solution (other liquid phases) or a highly insoluble protein fibril (solid phase). The soluble oligomers could be more cytotoxic and have the potential for intra- and intercellular permeability, which could also be able to form a membrane-embedded cytotoxic pore.[26−32] Thus, a deeper understanding of conformation adaptability of the protein in the early oligomeric states and the understanding of residue-specific changes in the course of protein fibrillation are still matters of investigation and targets for developing therapeutics.

The topology and morphological appearances of phase-separated oligomeric states can partially be visualized using atomic force microscopy (AFM) and electron microscopy (EM).[33,34] However, detailed residue-specific changes including the structural and molecular rearrangement are still challenging even by engaging advanced structural biology tools such as NMR and single-particle cryo-EM analysis.[35−39] In this article, using Raman spectroscopy, we delineate the crucial conformation state and the status of some of the important residues in the processes of fibril formation, and we considered bovine insulin (BI) as the model globular protein for the investigation of residue-specific changes and variation of Raman marker bands.

The native monomeric structure (Protein Data Bank (PDB) ID: 2ZP6) of BI consists of chain A (21 residues) and a 30-residue-long B-chain linked together by a pair of interchain disulfide bonds (Figure 1).[40−42] A-chain of the protein, however, contains an intrachain disulfide linkage at residues (C6−C11).[43,44] The A-chain contains an N-terminal α-helix (I2−A8), a noncanonical turn along with residues (S9−S12), and a C-terminal α-helix starting with residues (L13−Y19). The B-chain contains an α-helical fold in the central region (G8−V19), a β-strand (G24-Y27), and a disordered C-terminal region (T28−A30).[44,45] BI primarily adopts three helical segments constituting the enzyme's active form, and therefore, protein is primarily enriched with α-helical folds in its core geometry.[46] Insulin is found in deficient levels in the bloodstream as a monomeric unit which is the physiologically active form.[47] At higher concentrations, it easily converts to dimers at neutral pH and assembles into hexamers in the solution in the presence of zinc ions.[48] It has also been observed that the protein undergoes a conformational change and partial unfolding during the receptor binding process. Another important event that connects directly to the stability and compactness of the insulin monomer is the helical folds, which have a natural propensity to form insoluble fibrils in solutions; a related medical condition is called amyloidoma.[46] It is a pathological condition in patients with diabetes where insulin fibril accumulation occurs at the common insulin injection sites, causing a poor penetration of the injected hormone.[49,50] The fibril formation propensity could be further enhanced at low pH, high temperature, and low-to-moderate concentrations of a denaturing agent, e.g., Gdn-HCl, urea, and different salt concentrations.[51−58] Our investigation is directed to realize these events under Raman spectroscopy and to reveal some of the Raman signatures of the protein in its course of oligomeric phase separation and subsequent hydrophobic zipping and fibril formation.

We delineated the major Raman signature of the protein in its native-like folded monomeric state and the oligomeric and fibrillar conditions. It has been found that the Raman intensity ratio of the Fermi doublet (Raman bands) of tyrosine residues remained almost constant and indicated less perturbation of the hydrogen bonding nature of the residues in different phases of fibril formation. However, the conformational heterogeneity of the disulfide linkages was reduced. The current investigation also firmly established that the weak but definite Raman band at ~935 cm^{-1} appeared to be a golden standard and critical physical parameter to monitor highly complicated protein aggregation pathways and to investigate the liquid phase-

https://doi.org/10.1021/acsphyschemau.3c00065
ACS Phys. Chem Au 2024, 4, 268−280

separated oligomeric states of structured and intrinsically disordered proteins.

RESULTS AND DISCUSSION

This investigation used off-resonance Raman microscopy, fluorescence, and AFM imaging to investigate the protein conformation and residue-specific Raman spectroscopic details of BI in its course of fibrillation at an elevated temperature (60 °C). A fresh solution of BI (2 mg/mL) was prepared in an acidic buffer (25 mM HCl with 0.1 M NaCl, pH 1.6). The solution was subsequently incubated at 60 °C for several hours. The formation of protein oligomers and other aggregates was monitored initially by the measurement of steady-state fluorescence of thioflavin T (ThT) dye in the presence of an incubated protein solution. Figures 2 and S3 show the ThT fluorescence profile that represents the kinetics and spectral format of the amyloid fibril formation of BI. The fluorescence of ThT solution increases in the presence of β-sheet-rich protein fibrils. The plot of fluorescence intensity of ThT in the presence of protein solution incubated for different times against the time of incubation indicated typical sigmoidal growth kinetics of the fibril formation. There was an initial 50 min interval (lag phase) with no major changes in ThT fluorescence. Subsequently, the fluorescence intensity rapidly reached the maximum as the fibril formation equilibrium was reached. The measured growth rate, as reflected in $t_{1/2}$, was approximately 68 min.

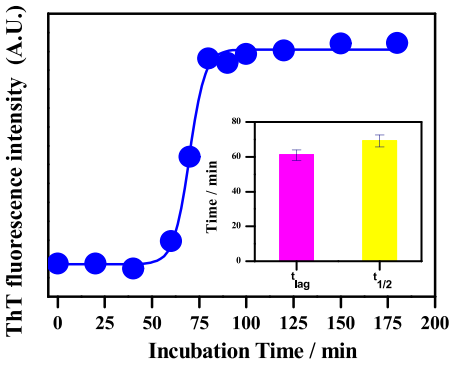

Figure 2. Amyloid fibril formation kinetics of BI monitored by the amyloid-specific binding of extrinsic fluorophore ThT. Each data point in the blue curve indicates the fluorescence intensity (at 482 nm) of ThT solution in the presence of the quantitative amount of aliquots of bovine insulin measured at different time points of incubation. ThT fluorescence was measured at an emission maxima of 482 nm and excited at 440 nm. Inset shows two kinetic parameters, t_{lag} and $t_{1/2}$, as obtained by fitting the data points (blue curve).

AFM was further used to confirm the nature of possible protein assembly states at different time points of the protein incubation (Figure 3). After 50 min of incubation (late lag phase), a heterogeneous mixture of small and large disk-shaped oligomers could be observed. The average height of these oligomeric species was 0.5−1 nm (Figure 3A). Interestingly, the ThT fluorescence did not substantially increase for these oligomeric species (Figure 2). After thermal incubation of the protein solution for approximately 70 min, the oligomer sizes slightly increased, and the presence of protofibrils was also noticed (Figure 3B). The average height was between 4 and 6 nm. At longer incubation times (80 min), considered as the late elongation phase, a significant distribution of protofibrillar aggregates could be observed as small thread-like structures, which typically ranged from 0.5 to 1 μm in length (Figure 3C). Figure 3D shows the formation of mature fibrillar aggregates after the protein sample was incubated for 120 min. The measured length was 1−3 μm.

The secondary structural changes during the early and late stages of aggregation have been probed using UV region circular dichroism (UV-CD) and confocal Raman spectroscopy.[59−66] The CD spectrum of the freshly prepared (before thermal incubation) BI in an acidic solution showed helix-predominant marker bands at ∼208 and ∼222 nm (black curve in Figures 4 and S4). It indicated that the protein solution

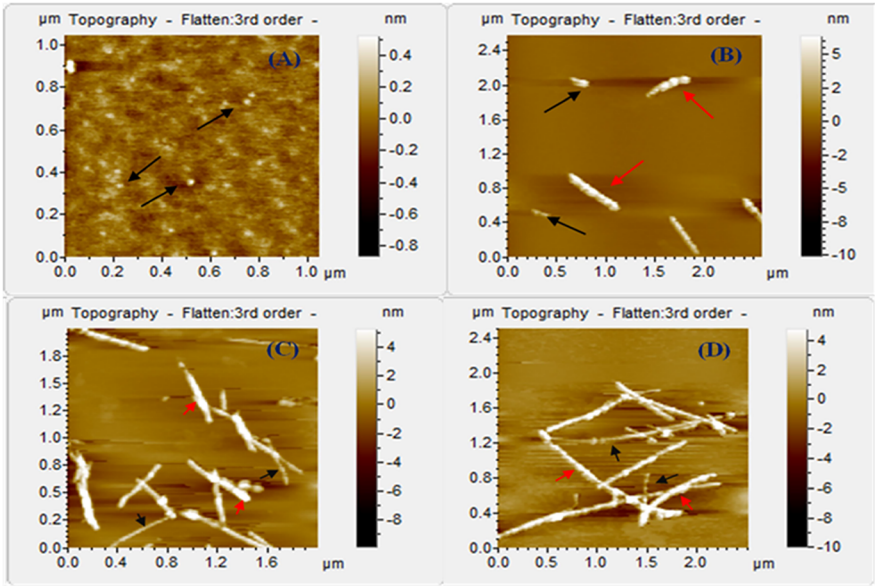

Figure 3. AFM images of BI aggregates produced at different time points of incubation. (A) Topographic view of heterogeneous oligomers (highlighted in black arrowhead) formed after incubation for 50 min. (B) Protofibrils with smaller widths (black arrowhead) produced after 70 min incubation period of the protein solution. The average height is 4−6 nm. (C) Coexistence of both small and long elongated protofilaments (80 min). (D) Images of quite mature bovine insulin fibrils 1−3 μm in length as identified in the stationary states (incubation time 120 min).

https://doi.org/10.1021/acsphyschemau.3c00065
ACS Phys. Chem Au 2024, 4, 268−280

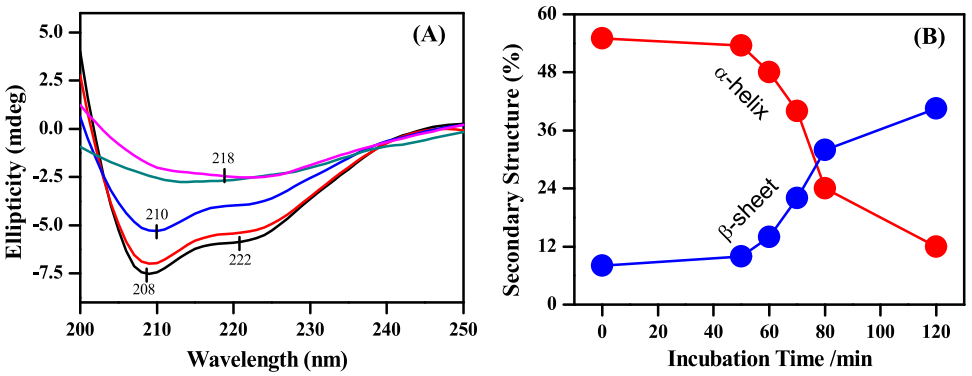

Figure 4. UV region CD analysis and major secondary structural rearrangements in the course of bovine insulin fibrillation. (A) Black line represents the CD spectra of BI freshly prepared in acidic buffer (HCl/NaCl) just before incubation (0 min) at a high temperature. Similarly red line is the CD spectra of oligomeric state taken after incubation for 50 min. Blue is obtained from mixtures of oligomers and protofilaments, and incubation time was 70 min. Green line obtained from the protein solution kept for 80 min incubation. Pink line is the representation of fibrillar entity obtained after 120 min of incubation. (B) Changes in the secondary structural components (α-helix and β-sheet) (%) against incubation time of BI in an acidic buffer led to the formation of different amyloidogenic aggregated states: helix (red) and sheet (blue).

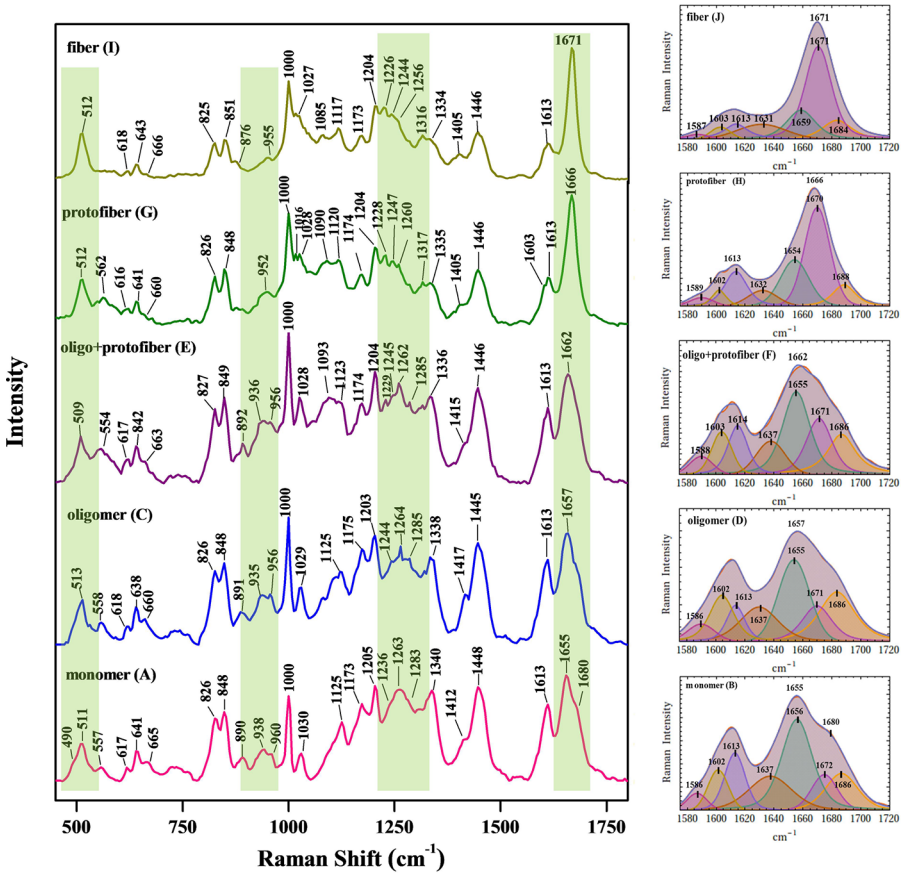

Figure 5. 532 nm laser-excited Raman spectra of BI at different time points incubation in acidic buffer. The regions 470−1800 cm^{-1} are shown. Incubation condition: [BI]: 2 mg/mL, 25 mM HCl with 100 mM NaCl buffer, pH 1.6, incubation temperature 60 °C. Raman spectra: (A) 0 time of incubation, monomer; (C) 50 min after incubation (oligomers are formed); (E) 70 min incubation (oligomer and protofilaments); (G) 80 min incubation (protofiber); (I) 120 min incubation (fiber). For each measurement, 20 μL protein solution was dropped and cast onto a glass coverslip for laser excitation, laser power at source 20 mW, ∼5 mW at the sample, recording time of 100 s. The displayed spectrum was an average of three or four scans, and a suitable baseline correction was made. Highlighted boxes indicate major changes in the peak pattern/intensity. Different panels on the right hand side show the curve fitting analysis of the amide I region (1575−1720 cm^{-1}) of the spectra shown on the left side (as stated above). (B) Monomer, (D) oligomer, (F) mixture of oligomer and protofiber, (H) protofiber, and (I) fiber. The band fitting protocol is described in Materials and Methods section. The orange and blue lines are the experimental and fitted spectra, respectively. Four component bands representing amide I regions are shown in green (α-helix, ∼1655 cm^{-1}), orange (loose β-strand and PPII and disordered, 1686 cm^{-1}), violet (β-sheet, ∼1671 cm^{-1}), and maroon (vibronic coupling bands, ∼1637 cm^{-1}). The peak positions are also fitted for aromatic residues: Tyr, ∼1613 cm^{-1}; Phe ∼1605 cm^{-1}, and unknown, 1586 cm^{-1}. A partial assignment of the Raman spectra is given in Table 1.

https://doi.org/10.1021/acsphyschemau.3c00065
ACS Phys. Chem Au 2024, 4, 268−280

Table 1. Partially Assigned Raman Vibrational Bands (cm^{-1}) of BI in Its Self-Assembled Oligomeric, Oligomer+ Protofilament, Protofiber, and Fibril States

BI at pH 1.6	oligomer	oligomer+ protofilament	protofiber	fiber	modes of Raman vibration
511	513	509	512	512	S−S
557	558	554	560		S−S
617	618	617	616	619	Tyr
641,670	638,660	642,663	641,677	643,666	C−S, Met
826,848	826,848	827,849	826,848	825,851	Tyr
890,938	891,935	892,936			C_α−C stretching (α-helix)
1000	1000	1000	1000	1000	Phe
1030	1029	1028	1028	1027	Phe
1125	1125	1123	1120	1117	CH_2 symmetric rock+ Cα−C streching
1205	1202	1204	1204	1204	Tyr, Phe
		1229	1228	1226	Type II β-turn, strand, Amide III
	1244	1245	1247	1244	
	1254			1256	Poly L-proline, Amide III
1263,1283	1264,1274	1262	1260		α-helix, Amide III
1340	1338	1336	1335	1334	Tyr
1448	1445	1446	1446	1446	CH_2, CH_3, and CH deformation and scissoring
1613	1613	1613	1613	1613	Tyr aromatic vibration
1655	1657				α-helix, Amide I
		1662	1685		Extended PP II
			1666		Extended PP II, β-sheet
				1671	β-sheet, Amide I

initially maintained a predominant α-helical secondary structure. The CD signature for oligomeric and protofibril states of the protein as produced by thermal incubation showed retention of most of its α-helical nature, and clear marker bands at ∼208 and ∼222 nm were clearly observed. The protein conformations embedded into the late protofilaments and mature fibrillar states changed to the β-sheet and it was confirmed with a spectral minimum at 218 nm. This observation revealed that freshly prepared insulin could rearrange its secondary structure from α-helix to a β-sheet structure during its micrometer-scale superstructures into an amyloid filament. The evolution of secondary structural reorganization suggested that the BI converted primarily its native α-helical conformation to β-sheet-enriched conformation during the fibrillation process (Figure 4B). The processes of fibrillation were similar to aggregation of human insulin (HI); however, the aggregation kinetic parameters appeared slightly different.

To further delineate the detailed conformational and secondary structural changes at different stages of aggregation and also to establish the Raman signature of different assembly structures and phase-separated entities, off-resonance Raman measurements were carried out on incubated protein samples. Figure 5 shows the Raman spectra (470−1800 cm^{-1}) of BI monomer and different types of aggregates produced in the course of protein fibrillation. Table 1 lists the peak positions and their association with different groups related to these vibrational (Raman) bands. Figure 5A shows the Raman spectrum of freshly prepared (zero time of incubation) BI and a broad amide I band could be seen at ∼1655 cm^{-1} having the full-width at half-maximum (fwhm) of ∼48 cm^{-1}. The peak was broadened at 1680 cm^{-1} (Figure 5A). The bands at 1655 and 1680 cm^{-1}, respectively, represent the α-helical secondary conformer and disordered state of the amide backbone, whereas the amide III region (1230−1300 cm^{-1}) was also predicted to have a predominant α-helical marker band.[63,66] The peak at 1263 cm^{-1} in the assigned amide III band corresponds to the α-helical restraint in the protein structure. The amide III band at 1283 cm^{-1} could correspond to the protein 2.5_1-helix conformation, which is structurally similar to poly-L-glutamic acid (PGA).[62,63,66]

In the oligomeric state of the protein, the amide I band at 1657 cm^{-1}, having an fwhm, of ∼45 cm^{-1} assigned for α-helical regions of the protein (Figure 5C). The amide III region of the Raman spectra of oligomers contains major bands at 1264 and 1285 cm^{-1}. The amide III bands of the Raman spectra of oligomer also showed two overlapping bands; the band at 1244 cm^{-1} is assigned to the polyproline II (PPII) state, and another band at 1254 cm^{-1} could be assigned as a signature for 3_{10}-helix.[67] A comprehensive analysis of the amide I and amide III bands and their respective peak positions could have suggested that a minimal secondary structural rearrangement had occurred inside the BI backbone when it transformed into the water-soluble oligomeric phase.

A sample containing a mixed population of oligomers and protofilaments, formed after a prolonged (70 min) incubation of the protein solution under identical conditions, had corresponding amide I Raman bands emerging at around 1662 cm^{-1} (Figure 5E and Table 1), which indicated a substantially increased disorder conformation, along with a decline of the helical state of the protein. The assigned bands at 1262, 1285, and 1245 cm^{-1} in amide III vibration correspond to the α-helical secondary structure and random coil state of the protein, further suggested to retain heterogeneous structural contents. A geometrical transformation into protofibrils and subsequent fibril development significantly altered the protein Raman signature. Figure 5G exhibited the Raman spectrum of BI protofiber. Amide I Raman spectra at 1666 cm^{-1} had identified both the disorder and β-sheet-enriched structure located in protofilament species (Figure 5G and Table 1). However, the confocal Raman spectrum of BI filaments showed a pronounced change in the intensity and sharpness of the amide I peak at 1671 cm^{-1} (Figure 5I and Table 1). The narrow and sharp amide I band

https://doi.org/10.1021/acsphyschemau.3c00065
ACS Phys. Chem Au 2024, 4, 268−280

Table 2. Secondary Structural Components of BI in Its Different Self-Assembled States Are Shown as a Percentage of the Total Band Area (%A)[a]

species (self-assembled states)	α-helix			β-sheet			β-strand, PPII, and disordered			disordered/vibronic coupling bands		
	peak (cm^{-1})	%A	width (cm^{-1})	peak (cm^{-1})	% A	width (cm^{-1})	peak (cm^{-1})	%A	width (cm^{-1})	peak (cm^{-1})	%A	width (cm^{-1})
BI at pH 1.6	1656	49	30	1674	12	29	1686	18	24	1637	20	32
oligomer	1655	41	30	1670	15	28	1684	24	27	1630	20	32
oligomer+ protofilament	1655	37	26	1671	30	27	1686	18	25	1637	14	35
protofilament	1654	28	25	1671	41	22	1685	12	24	1632	10	31
fiber	1659	19	24	1671	54	20	1684	12	23	1631	15	30

[a]The respective component peak position (cm^{-1}) and relative spectral bandwidth (%A) of each fitted component are shown in the table.

at 1671 cm^{-1} (fwhm, 20 cm^{-1}) is assigned to a well-ordered cross β-sheet secondary structure of a protein molecule.[68] The corresponding amide III region was composed of a significant band of 1226 cm^{-1} that also supported the presence of cross β-sheet conformation in fibrillar states.[69] The other two amide III peaks at 1244 and 1256 cm^{-1} were observed at the shoulder position, which corresponds to the random coil and 3_{10}-helix conformations, respectively. Therefore, filament states could also be associated with a partial random coil and 3_{10}-helix conformation along with a predominant cross β-sheet structure.

Different panels at the right position in Figure 5 showed the results of the component fit analysis of the amide I Raman band and a semiquantitative estimation of the secondary structures present in different assembly states of the protein.[60−63,65,66,70] The amide I region (1575−1720 cm^{-1}) curve fitting and multicurve analysis were performed using Gaussian and Lorentzian algorithms.[60−63,65,66] This region consists of four component bands that are linked to different forms of secondary protein structures. The estimated results of these curve fitting analyses are given in Table 2. In a monomeric state, the amide I component band at 1656 cm^{-1} predicted the content of ∼54% α-helical domain (Figure 5B and Table 2).[63,66] However, a significant quantity (∼24%) of random coil structure was also evidenced and assigned to a component band at 1686 cm^{-1}.[63,66] An imperceptible β-content of 9% was derived from the respective component band area at 1672 cm^{-1}. However, the crystal structure of BI also contained a similar secondary structural evolution (50−52% of residues belong to the α-helical region in the Ramachandran area, and 12% of the structure contained β-sheet-enriched residues).[71] In the oligomeric state, 41% of amino acid residues had predicted retained the α-helical signature, as identified for the component amide I band at 1655 cm^{-1}. A considerable amount (∼24%) of random coil structure was further identified for the assigned component band at 1686 cm^{-1}. An imperceptible β content of 15% was derived from the amide I component band area at 1671 cm^{-1} in the oligomeric states present in the lag phase of fibrilization (Figure 5D and Table 2). The details of the secondary structural component analysis for the mixed oligomer and protofilament state are shown in Figure 5F and further depicted in Table 2. In these mixed oligomeric and protofilament states, the overall α-helical content with the component band at position 1655 cm^{-1} declined to 37% with the component band at position 1655 cm^{-1}. Whereas the β-sheet content increased to 27% (component amide I band at 1671 cm^{-1}), and PPII-like conformation or unordered content remained at 25% with the signature band at 1686 cm^{-1}. The Raman spectra of protofiber were identified with the appearance of both unorder and β-sheet structures as identified from a marker band of the amide I region at 1666 cm^{-1} (Figure 5G and Table 2). In this course of evolution of large polymerized species, the helical content decreased dramatically and was finally confined to 28% (component band at 1654 cm^{-1}), while the β-strand/sheet content increased up to 41% (component band at 1670 cm^{-1}) (Figure 5H). The narrowed and sharp vibrational amide I band at 1671 cm^{-1} (20 cm^{-1}) in the spectra of fibrillar BI was assigned to the cross β-sheet structure. In this fibrillar species, the helical content was finally decreased to 19% (component band at 1659 cm^{-1}), while the β-strand/sheet content was increased by 54% (component band at 1671 cm^{-1}), and unordered or PPII conformation was also decreased to 12% with its signature amide I band at 1684 cm^{-1} (Figure 5J and Table 2).[61,63,72] Figure 6 represents the overall rearrangements in the secondary structural elements of different intermediate species, as obtained from our Raman spectroscopic analysis suggested that α-helical conformation significantly decreased throughout the insulin amyloid process, although extended conformations (PPII, extended helix) persisted until full amyloid fiber was formed.

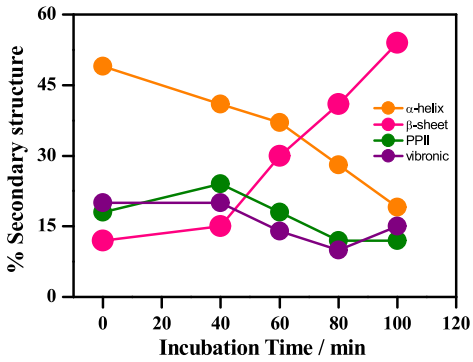

Figure 6. Time-correlated changes in the secondary structural components of incubated bovine insulin, as obtained from the curve fitting analysis of the Raman amide I band. Color key: orange, helix (1655 cm^{-1}); pink, β-sheet (1671 cm^{-1}); green, loose β-strand and PPII and disordered (1686 cm^{-1}); and violet, vibronic coupling bands (∼1637 cm^{-1}).

The Raman spectra of the samples after 0 and 50 min of incubation looked highly similar (Figure 7A). The Raman spectra were normalized by adjusting the intensity of the phenyl band at 1000 cm^{-1} since the intensity of aromatic ring breathing of phenylalanine intensity at 1000 cm^{-1} had a minor impact on visible light (532 nm) excitation.[73−76] A slight widening of the amide I band suggested an increase in

https://doi.org/10.1021/acsphyschemau.3c00065
ACS Phys. Chem Au 2024, 4, 268−280

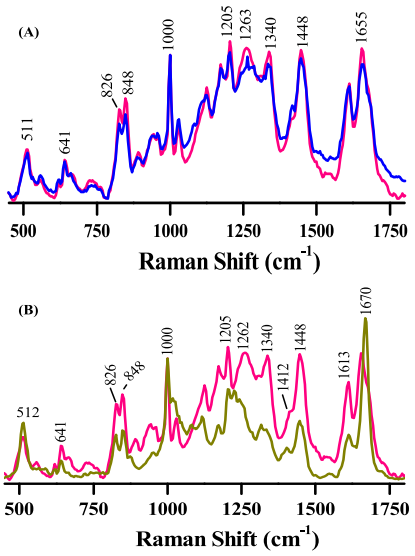

Figure 7. Comparison of Raman spectral signatures between different self-assembled species. (A) Variations in the averaged Raman spectra (470−1800 cm^{-1}) of monomeric bovine insulin at pH 1.6 (red) and its self-assembled oligomers (blue). (B) Comparison of Raman spectra (475−1800 cm^{-1}) of monomer (pink) with that of the mature filament (greenish yellow).

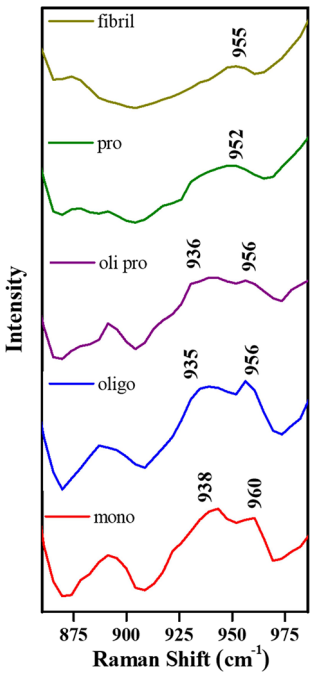

Figure 8. Observed data illustrate changes in the Raman intensity of the distinct helical marker band located at 940 cm^{-1} across various time intervals of incubation. Sample preparation and other conditions are the same as shown in Figure 5.

fluctuation in the conformation and/or its dynamics. The amide III area also exhibited slight broadening and variations in Raman intensity.[73,76] However, a distinct and opposite variation (decrease in Raman bandwidth in the fibril state) was particularly visibly noticeable in the comparison of the 0 min incubation samples, and the fibrils recovered after 120 min (Figure 7B). Therefore, it was suggested that significant conformational changes occurred during fibrilization in the presence of a major positive band at 1651 cm^{-1} and a negative peak at 1670 cm^{-1} in the amide I region. Also, a negative difference spectra characteristic of 1225 cm^{-1} revealed a strong β-sheet structure. However, in the oligomeric state (50 min incubation), broadening may be linked to partial unfolding and formation of molten globule-like conformation that may aid in the initiation of fibril formation.

In the low-frequency region (fingerprint region) of Raman spectra, 900−1000 cm^{-1} is sensitive to a protein's side chain residues and tertiary structural movements.[77] The helical signature peak in the fingerprint region had previously been characterized at (930−940 cm^{-1}), whereas the β-stand and disordered structural content were identified at (980−990 cm^{-1}) and 960 cm^{-1} respectively.[60,62,63,65,69,77−79] The Raman bands for monomeric BI at pH ∼1.6 appeared at ∼938 cm^{-1} suggesting its α-helix conformation, while a peak at 960 cm^{-1} was referenced for the disordered segments. In addition, low-frequency backbone conformation signals at 935 and 956 cm^{-1}, which exist for the helix and disorder conformations, respectively, were also present in the BI oligomeric states. The protofilament states were accompanied by the Raman band at 954 cm^{-1}, suggesting that the BI protofilament region was enriched with a disorder conformation. After prolonged incubation, while protofibrils converted into their mature filament stages, a noticeable change (intensity and sharpness) of this disordered band position at 957 cm^{-1} occurred (Figure 8).

In the journey of BI amyloid formation, we observed a decrease in the helical conformation and a concomitant increase in the β-sheet structure of the protein. A contemporary study by Thomas et al. stated that the Raman band near 1338−1342 cm^{-1} was a marker for the α-helical secondary structure.[80] We also noticed a signature band at 1338 cm^{-1} in the oligomeric state, denoting its α-helical geometry.[70,80] The band intensity at 1338 cm^{-1} had significantly reduced in the amyloid fibrillar state, confirming the significant loss of helical conformation prior to conversion into a β-sheet-shaped fibrillar state. However, it was important to note that complete loss of Raman intensity at ∼1340 cm^{-1} did not happen, and it could be due to loss of α-helical secondary structure. The Raman band at 1448 cm^{-1} in the monomer state, assigned for CH_2−, CH_3− deformation, and CH_2− scissoring motion had shifted to a lower frequency and became sharper in the protofilament and fibrillar states.[69] This also suggested a dramatic conformational rearrangement in the protein backbone and side chain vibrations of the individual residues of BI. In the processes of fibrillation, it was confirmed that the protein secondary structure was enriched with β-sheet; however, no significant downshift at 1446 cm^{-1} Raman band could be observed when protofilament reached fibrillar states.

Tryptophan and tyrosine are two important residues responsible for protein folding/misfolding and maintaining hydrophobic clustering inside protein core geometry.[81−83] Thus, the alteration of their microenvironment could significantly reduce the folding and stability of any reference protein. BI contains four tyrosine residues that remain exposed outside the core folded geometry.[83] The ratio of Raman intensities I_{850}/I_{830} (tyrosine Fermi doublet) generally serves as a molecular marker of hydrogen bonding behavior and strength between the phenyl−OH group with bulk solvent molecules. In the oligomeric state, the tyrosine Fermi doublets peak position and intensity remain unchanged. However, the Fermi doublet's intensity has reduced in protofiber species, and the referenced ratio of Fermi doublets 1.1 suggested a relatively

https://doi.org/10.1021/acsphyschemau.3c00065
ACS Phys. Chem Au 2024, 4, 268−280

weaker hydrogen bond strength. Following the mature fibers formation, the tyrosine Fermi doublet ratio became 1.0. This implied the further weakening of H-bonding between the tyrosine−OH moiety and surrounding water molecules prior to formation of β-sheet conformation. Therefore, the resulting tyrosine residues could get slightly buried inside the hydrophobic core of β-sheet structure during its aggregation into amyloid fiber.

Tyrosine had also been reflected in its aromatic C═C stretching vibration at ∼1612 cm^{-1}. Both the amide I region of the Raman spectra and the relative Raman difference spectra suggested the downshift of this peak, which primarily reflects a partial, gradual weakening of H-bond strength. This observation was further supported by the quenching study of intrinsic tyrosine autofluorescence measured at different time intervals. The gradual decrease in the tyrosine fluorescence intensity, as observed during the aggregation process, is shown in Figure S1. The inverse sigmoidal tyrosine autofluorescence curve demonstrated that the structural rearrangement from monomer to oligomeric state, including tyrosine side chain reorientation, occurred slowly (in the lag phase). While the oligomers transform into protofibrils, the fluorescence of tyrosine decreases significantly. At 80 min of incubation (during ongoing protofibril generation), the tyrosine fluorescence intensity dropped significantly, indicating that tyrosine residues might entered the hydrophobic pockets of the misfolded protein assembly. However, the relative quenching of fluorescence intensity remained static during filament formation, had further indicated that the buried nature of tyrosine residues within the hydrophobic pockets inside the protein assembly remains unchanged in both protofilament and fibrillar states of the protein. Such quenching of tyrosine fluorescence could arise due to its interactions with sterically zipped side chain residues, suggesting that the tyrosine side chain could take part in steric zipper formation in the BI fiber structure.

Raman spectroscopy may reveal the secondary structural details of proteins in various forms including soluble oligomers and insoluble fibrillar aggregates. The asymmetric amide I vibration bands that appear in the range of (1650−1680 cm^{-1}) in Raman spectra of proteins and peptides represent C═O stretching, and a small contribution of out-of-phase C−N stretching of the amide backbone, the amide II vibration (1550 cm^{-1}) consists of an out-phase mixture of C−N stretching and N−H bending motion, amide III (1200−1350 cm^{-1}), which involves C−N stretching and N−H bending.[84,85] These bands provide ample conformation states of the protein in different forms of the proteins. We recently developed a quantitative estimation of the secondary structure of natively unfolded proteins using a four-component Raman amide I band fitting. Studies on the in vitro aggregation of insulin have shown the development of soluble oligomeric intermediates, commonly termed protofibrils, which dissolve upon fibril formation. We used a combination of Raman microscopy and AFM to examine the aggregates created in vitro to more thoroughly define the structural changes that occur during BI aggregation. Most of the structural analysis of amyloid fibrils made from different proteins has been done on assemblies in vitro or extracellular deposits. These fibrils underwent X-ray fiber diffraction investigations, identifying a similar cross-β structure with β-strands parallel to the fibril axis.[54] Studies using the Fourier-transform infrared spectroscopy (FT-IR) and solid-state nuclear magnetic resonance (NMR) showed that the amyloid fibrils have parallel and antiparallel β-sheet orientations.[58,86] The structure of amyloid fibrils has been studied by using various spectroscopic techniques, and researchers are making steady progress in this work. A complete lack of structural information regarding the intermediates formed during fibrillization: our data reveal that the oligomers formed by incubation time at 50 min retain a significant amount of 41% of α-helical signature and percentage random coil structure (∼24%) of random coil structure and 15% β content structure. Furthermore, a significant extent to β-structure conversion and a slight α-helix to β-structure transition occur when protofilaments are formed.

Disulfide linkages play a critical role to maintain the stability and physiological functions of a protein.[87,88] The conformations of disulfide bonds decide the tertiary and secondary structure of the protein, and Raman spectroscopy is a useful way to monitor the helical structure of the protein and transform it to the β-sheet conformation of disulfide bonds in situ and in real time. The native state of BI the S−S frequencies of the three disulfide linkages appeared at position ∼513 (ggg), ∼530 (ggt), and ∼545 (tgt) cm^{-1} (Figure 9).[72,89,90] Freshly prepared BI produced Raman frequencies at

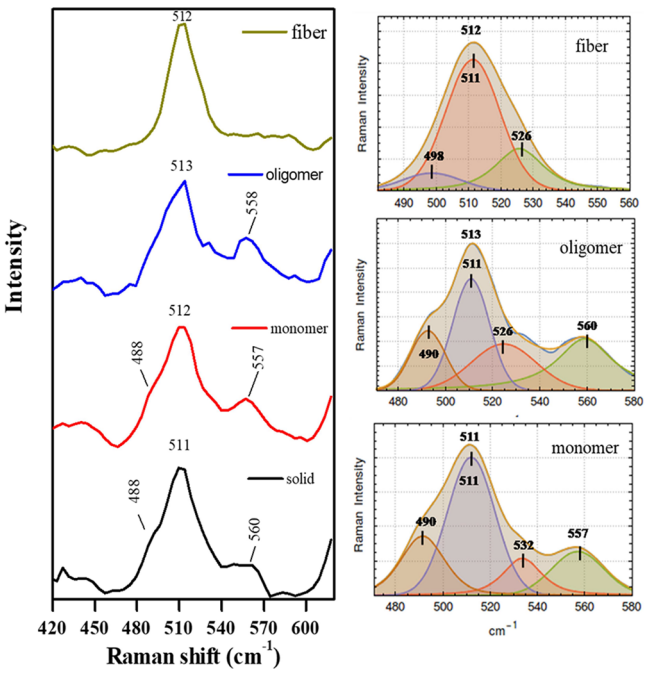

Figure 9. Raman spectra of BI over the spectral region of 420−630 cm^{-1} representing mainly the S−S disulfide mode of vibrations. Apart, from solid sample, the other experimental conditions were the same as in Figure 5. The right panels show the respective Raman band decomposition (regions 470−580 cm^{-1}) using a Gaussian/Lorentzian function with a maximum fwhm of 30 cm^{-1}.

511, 530, and 545 cm^{-1} due to the R−S−S−R linkages assigned to ggg, ggt, and tgt geometries, respectively. The band frequencies remained mostly unchanged, however, slightly broadened in the oligomeric phase of insulin fibril formation pathway. For longer incubation of the protein, the S−S bond frequency became much narrower and the asymmetry nature was mostly abolished in the fibrillar state. In this state, it showed only one disulfide Raman band at ∼512 cm^{-1}. The geometry of the interchain disulfide bonds (B7-A7 and B12-A20) in the fibrillar phase may be also realigned to "ggg"

https://doi.org/10.1021/acsphyschemau.3c00065
ACS Phys. Chem Au 2024, 4, 268−280

orientation, similar to intrachain disulfide conformation, and the band position remained at 512 cm^{-1}. This spectral finding corroborated with other events such as preservation of most of the protein secondary structure in the oligomeric state and its elevation to formation of highly stable β-sheet structure in the fibrillar state of the protein aggregates. We also conducted quantitative assessments to examine the extent of disulfide bond cleavage when analyzing heated samples in comparison to normal samples, as depicted in Figure S5. The results demonstrate that the Raman intensity of disulfide bonds did not significantly decrease. To ensure accurate measurements, we normalized the Raman spectra against the phenylalanine band at 1003 cm^{-1}. Although there may be some protein loss during the aggregation processes, it is deemed insignificant and can be disregarded.

During the formation of BI fibrillation, the α-helical content is reduced significantly (19%), and the proportion of β-sheet structure increases (54%), while the contribution of extended and PPII in fibrillar assembly was minimal, the Raman intensity of the shoulder band at ∼1680 cm^{-1} was reduced significantly. However, in the oligomeric phase, most of the protein conformations were preserved. These secondary structural data demonstrated that, on aggregating into oligomers under acidic conditions, a significant change in the ensemble of structures present takes place in the fibrillar phase, the β-sheet structure is enhanced, and the disordered secondary structure is diminished. Importantly, oligomeric BI maintained its α-helical space, and the fluctuation level may be similar to the monomeric state of the protein. The Raman band at ∼935 cm^{-1} is an important α-helical marker for the oligomeric status. We showed the band present in BI Raman spectra in the oligomeric and monomeric states. We also observed the band in egg-white lysozyme at ∼935 cm^{-1}.[62] Further, we noticed the band present in the α-synuclein oligomer (Figure S2). Small-angle X-ray scattering and computational modeling studies have indicated that insulin oligomers were found to be α-helical conformation.[91] Hayden and Teplow showed that Aβ oligomeric intermediates that include a considerable amount of α-helix and the formation of fibrils result in a significant conversion of α-helix to β-structure.[92] However, most of the Raman band, including the disulfide marker band at ∼513 cm^{-1}, was slightly broadened and indicated distorted geometry during the formation of the oligomeric assembly structure. Compared to monomeric and oligomeric samples, a substantial amount of homogeneity in disulfide (−S−S−) linkages was observed, and predominantly the Raman band at 512 cm^{-1} remained in the fibrillar state. The tyrosine Fermi doublet at I_{850}/I_{830} was slightly decreased; however, the bands became sharper. It is pertinent to mention that the spectral nature (baseline) in this region may have an adverse effect on the calculation of the intensities of the tyrosine Fermi doublet. Overall, the data indicated that in the fibrillar state compared to its oligomeric condition the tyrosine microenvironment became more hydrophobic in the fibrillar state, and the hydrogen bonding nature of the tyrosine may, however, not change significantly.

SUMMARY AND PERSPECTIVES

Phase separation of soluble globular or intrinsically disordered protein to another soluble protein phase (soluble oligomer) and insoluble solid phase (fibrils) is a key event during the formation of quite stable and highly ordered protein aggregates. This phase separation and associated protein conformation change phenomena are linked to several pathological conditions for human diseases. Slowly, it is assumed that the oligomeric state of several proteins and peptides could be causative factors of amyloid diseases. Oligomer-containing soluble phase in many instances also serves as functional amyloids and is a key for storage and function of several proteins and enzymes. However, structural and the residue-specific information on the oligomeric phage are very limited as techniques such as NMR and protein crystallography are insufficient to probe these large-size protein entities. Our previous Raman-based analysis and others observed that in the oligomeric state most of the proteins preserved intact or extended helical conformation. In this investigation based on Raman spectroscopic analysis, we further confirmed that in the oligomeric state, it retained most of its helical component; we showed that the α-helical Raman marker band remained at 935 cm^{-1} in the soluble oligomeric phase. Our investigation further revealed that the hydrogen bonding nature of the tyrosine residues remained quite similar, though the microenvironment became more hydrophobic in the fibrillar state. It was also shown that the conformational heterogeneity of the three disulfide linkages was mostly present in the oligomeric phase of the protein; however, it decreased significantly, and only the ggg conformation was predominately observed in the fibrillar state.

MATERIALS AND METHODS

Materials

BI was purchased from Sigma Chemical Co. (catalog number I6634). Milli-Q water (Millipore Ltd., Bedford, MA) was used in all experiments to prepare the samples. Thioflavin and tyrosine were obtained from Sigma-Aldrich. The stock solution of BI (2 mg/mL) was prepared freshly in NaCl/HCl solution of pH ∼ 1.6 (25 mM HCl containing 0.1 M NaCl). A stock solution of ThT was prepared, and concentration was checked using a molar extinction coefficient of 24,420 M^{-1} cm^{-1} at 420 nm. ThT was stored at 4 °C and protected from light for further use. Aliquots of the protein samples at specified intervals were collected and used for the spectroscopic analyses.

Sample Preparation for the Aggregation Study

Recombinant BI was dissolved in 25 mM HCl containing 0.1 M NaCl (pH ∼ 1.6) to make an initial stock protein solution of 500 μM and further centrifuged at 15,000 rpm for 10 min to remove the insoluble aggregates. The protein concentration was determined by measuring the UV absorbance of internal chromophore tyrosine at 278 nm on a JASCO 600 UV−visible spectrometer. The molar extinction coefficient of BI at 278 nm is 6080 M^{-1} cm^{-1}. The freshly prepared protein stock solution was diluted to 300 μM and incubated for several minutes at 60 °C without agitation. We further conducted ThT assays, AFM, and Raman spectroscopic investigations to monitor the formation of aggregated species during its incubation using the protein aliquots taken at various time intervals. The protein solution quality was confirmed by conducting Native gel electrophoresis on the incubated samples. Analysis of the Native gel image (Figure S6) depicted indications that some degradation and chemical alteration may have occurred.

AFM Imaging

AFM images were recorded in a Pico plus 5500 AFM (Agilent Technologies, Tempe, AZ, USA) with a piezo scanner over 9 μm^2. The aliquots of the incubated protein solution were collected at certain intervals and were diluted 10−50 times. Ten microliters of the diluted sample were then drop-casting on a freshly cleaved washed mica surface. After a few minutes, the sample was dried gently using airflow and washed with Milli-Q water to remove excess unbound proteins and undesired salt crystals. Microfabricated silicon cantilevers of 225 mm in length with a nominal spring force constant of 21−98 N

https://doi.org/10.1021/acsphyschemau.3c00065
ACS Phys. Chem Au 2024, 4, 268−280

m^{-1} were used from nanosensors. The cantilever oscillation frequency was turned into the 150−300 kHz resonance frequency. The tomographic images were further processed by flattening using Pico view software (Molecular Imaging Corporation, USA).

Raman Spectroscopy

Raman data were recorded using a commercial AIRIX Corp STR Raman microspectrometer equipped with a 532 nm semiconductor laser, 600 lines/mm diffraction grating, and a thermoelectrically cooled charge-coupled device (CCD) detector. The Raman bands were calibrated against the 519 cm^{-1} spectral line for silicon wafer. The semiconductor laser was focused on the sample through a microscope (Olympus BX51M, Japan) using a 50× objective lens. The backscattered Raman signal was also collected by the microscope. The power of the laser on the sample was ∼20 mW. Spectra were recorded over a spectral range of 400−4000 cm^{-1} region with a data acquisition time of 100 s. Five consecutive scans were averaged followed by baseline correction (multipoint baseline) and smoothening (Savitzky-Golay, 5 points) using Origin software.

Deconvolution of the Amide I Band

Amide I is a distinctive band in the protein Raman spectrum that can be used to study changes in the protein's secondary structure. Using Curve Fit's Levenberg−Marquardt nonlinear least-squares method, the Raman amide I deconvolution was carried out using GRAMS/AI 9.02 software packages. The amide I mode (1575−1720 cm^{-1}) of the Raman spectra was fitted using Gaussian and Lorentzian functions, including four asymmetrical components representing the four different secondary structural elements of BI: the component band 1655 cm^{-1} is assigned to the α-helical conformation with spectral window 1650−1660 cm^{-1}, the β-sheet component band near 1672 cm^{-1} (window 1670−1675 cm^{-1}), polyproline II and disordered structure near 1685 cm^{-1} (window 1680−1690 cm^{-1}), and disorder structure or vibronic coupling band near 1637 cm^{-1} (window 1630−1645 cm^{-1}). Three distinct bands were also added during amide I band fitting for the ring vibrational modes of phenylalanine and tyrosine at 1585, 1604, and 1615 cm^{-1}, respectively. Allowing for homogeneous and heterogeneous broadening and the band fitting for comparisons of the χ^2 values and a follow-up, the standard error for peak positions is <5 cm^{-1} and for peak widths <5 cm^{-1} with an uncertainty of measurements typically less than 10%.

ThT Fluorescence Assay

A stock solution of ThT dye (1 mM) was prepared in the MiliQ water and stored in the refrigerator at 4 °C. Concentration of stock ThT dye was determined considering a molar extinction coefficient of 36,000 M^{-1} cm^{-1} at 412 nm. To monitor amyloid fibrillation, 500 μL of ThT solution (22 μM) was taken, and a 10 μL of incubated BI solution (6 μM) was pipetted out and appropriately mixed. In addition, the following parameters were adjusted for monitoring ThT fluorescence intensity during the aggregation experiment: Emission spectra were acquired over the wavelength range of 450 to 600 nm using an excitation wavelength of 440 nm; excitation and emission slits were 5 nm each. Fluorescence intensity was monitored at an emission maximum of 482 nm.

CD Spectroscopy

The far-UV-CD spectra of the BI samples were recorded with a JASCO J-815 CD spectropolarimeter at room temperature. A freshly prepared BI (300 μM) solution was incubated at 60 °C without agitation for CD analysis. The samples collected at certain time intervals were diluted to 10 μM and transferred to a quartz cuvette of a path length of 1 mm path length. The CD spectra were recorded over the spectral range of 195−250 nm with a scanning speed of 50 nm/min and a resolution of 0.2 nm. For each sample, three consecutive scans were averaged. For each sample, the representative spectrum was an average of at least three individual scans.

Tyrosine Fluorescence Assay

The incubated protein stock solutions used for UV-CD, AFM, and Raman spectroscopic studies at different time intervals were further taken for tyrosine autofluorescence measurement. The intrinsic tyrosine autofluorescence assay was recorded between 285 and 350 nm using an excitation of 278 nm for a diluted protein concentration of 8 μM using a fluorescence spectrometer (CARY Eclipse, VARIAN).

■ ASSOCIATED CONTENT

Supporting Information

The Supporting Information is available free of charge at https://pubs.acs.org/doi/10.1021/acsphyschemau.3c00065.

Fluorescence change during BI amyloid formation; Raman spectra of different species α-synuclein; ThT fluorescence emission spectra of BI fibrillation; CD spectra of BI; Raman difference spectra of BI fibrillation; and native-Page of BI (S6) (PDF)

■ AUTHOR INFORMATION

Corresponding Author

Nakul C. Maiti − *Structural Biology and Bioinformatics Division, Indian Institute of Chemical Biology, Council of Scientific and Industrial Research, Kolkata 700032, India;* orcid.org/0000-0002-8498-6502; Phone: +91-33-2499-5940; Email: ncmaiti@iicb.res.in

Authors

Sandip Dolui − *Structural Biology and Bioinformatics Division, Indian Institute of Chemical Biology, Council of Scientific and Industrial Research, Kolkata 700032, India;* Present Address: Eminent College of Pharmaceutical Technology, Barasat, West Bengal 700126, India (S.D.)

Anupam Roy − *Structural Biology and Bioinformatics Division, Indian Institute of Chemical Biology, Council of Scientific and Industrial Research, Kolkata 700032, India*

Uttam Pal − *Structural Biology and Bioinformatics Division, Indian Institute of Chemical Biology, Council of Scientific and Industrial Research, Kolkata 700032, India;* orcid.org/0000-0003-2110-4610

Shubham Kundu − *Structural Biology and Bioinformatics Division, Indian Institute of Chemical Biology, Council of Scientific and Industrial Research, Kolkata 700032, India*

Esha Pandit − *Structural Biology and Bioinformatics Division, Indian Institute of Chemical Biology, Council of Scientific and Industrial Research, Kolkata 700032, India*

Bhisma N Ratha − *Department of Chemical Sciences, Bose Institute, Kolkata 700091, India;* Present Address: School of Agricultural& Bioengineering, Centurion University of Technology and Management, Odisha, 761211, India (B.N.R.)

Ranit Pariary − *Department of Chemical Sciences, Bose Institute, Kolkata 700091, India*

Achintya Saha − *Department of Chemical Technology, University of Calcutta, Calcutta 700009, India*

Anirban Bhunia − *Department of Chemical Sciences, Bose Institute, Kolkata 700091, India;* orcid.org/0000-0002-8752-2842

Complete contact information is available at: https://pubs.acs.org/10.1021/acsphyschemau.3c00065

Author Contributions

S.D. conceptualized and designed the project. S.D. performed the experiments, analyzed the data, and drafted the manuscript. S.K. and E.P. assisted with the experiments. U.P. A.R. R.P. and

https://doi.org/10.1021/acsphyschemau.3c00065
ACS Phys. Chem Au 2024, 4, 268−280

B.N.R. helped with drafting the manuscript. A.S. and A.B. edited the manuscript. N.C.M. supervised the experiments with data analysis and corrected the manuscript. CRediT: **Sandip Dolui** conceptualization, data curation, formal analysis, investigation, methodology, project administration, software, validation, writing-original draft, writing-review & editing; **Anupam Roy** conceptualization, formal analysis, writing-review & editing; **Uttam Pal** software, visualization, writing-original draft, writing-review & editing; **Shubham Kundu** data curation, formal analysis, writing-review & editing; **Esha Pandit** formal analysis, visualization; **Bhisma N. Ratha** formal analysis, visualization, writing-review & editing; **Ranit Pariary** formal analysis, visualization; **Achintya Saha** writing-original draft, writing-review & editing; **Anirban Bhunia** visualization, writing-review & editing; **Nakul Chandra Maiti** conceptualization, formal analysis, project administration, resources, supervision, validation, writing-original draft, writing-review & editing.

Notes

The authors declare no competing financial interest.

■ ACKNOWLEDGMENTS

S.D. thanks CSIR network project BSC0113 and BSC0121 for funding support. S.K., E.P. thanks CSIR for the fellowship. The authors thank the Director and associates of the central instrumental facility of CSIR-IICB for providing all the instrument facilities.

■ ABBREVIATIONS

BI, bovine insulin; HI, human insulin; AFM, atomic force microscopy; ThT, Thioflavin T; CD, circular dichroism; CCD, charge-coupled device; PGA, poly-L-glutamic acid; PP II, polyproline II; fwhm, full width at half maximum; IDPs, intrinsically disordered proteins; UV-CD, ultraviolet circular dichroism; AFM, atomic force microscopy.

■ REFERENCES

(1) Dobson, C. M. Protein Folding and Misfolding. *Nature* **2003**, *426* (6968), 884−890.
(2) Chiti, F.; Dobson, C. M. Protein Misfolding, Functional Amyloid, and Human Disease. *Annu. Rev. Biochem.* **2006**, *75*, 333−366.
(3) Carulla, N.; Zhou, M.; Arimon, M.; Gairí, M.; Giralt, E.; Robinson, C. V.; Dobson, C. M. Experimental Characterization of Disordered and Ordered Aggregates Populated during the Process of Amyloid Fibril Formation. *Proc. Natl. Acad. Sci. U. S. A.* **2009**, *106* (19), 7828−7833.
(4) Lansbury, P. T. Evolution of Amyloid: What Normal Protein Folding May Tell Us about Fibrillogenesis and Disease. *Proc. Natl. Acad. Sci. U. S. A.* **1999**, *96* (7), 3342−3344.
(5) Soto, C.; Pritzkow, S. Protein Misfolding, Aggregation, and Conformational Strains in Neurodegenerative Diseases. *Nat. Neurosci* **2018**, *21* (10), 1332−1340.
(6) Selkoe, D. J. Folding Proteins in Fatal Ways. *Nature* **2003**, *426* (6968), 900−904.
(7) Uversky, V. N.; Fink, A. L. Conformational Constraints for Amyloid Fibrillation: The Importance of Being Unfolded. *Biochim. Biophys. Acta* **2004**, *1698* (2), 131−153.
(8) Yonezawa, Y.; Tanaka, S.; Kubota, T.; Wakabayashi, K.; Yutani, K.; Fujiwara, S. An Insight into the Pathway of the Amyloid Fibril Formation of Hen Egg White Lysozyme Obtained from a Small-Angle X-Ray and Neutron Scattering Study. *J. Mol. Biol.* **2002**, *323* (2), 237−251.
(9) Ross, C. A.; Poirier, M. A. Protein Aggregation and Neurodegenerative Disease. *Nat. Med.* **2004**, *10* (Suppl), S10−17.
(10) Willbold, D.; Strodel, B.; Schröder, G. F.; Hoyer, W.; Heise, H. Amyloid-Type Protein Aggregation and Prion-like Properties of Amyloids. *Chem. Rev.* **2021**, *121* (13), 8285−8307.
(11) Ashraf, G. M.; Greig, N. H.; Khan, T. A.; Hassan, I.; Tabrez, S.; Shakil, S.; Sheikh, I. A.; Zaidi, S. K.; Wali, M. A.; Jabir, N. R.; Firoz, C. K.; Naeem, A.; Alhazza, I. M.; Damanhouri, G. A.; Kamal, M. A. Protein Misfolding and Aggregation in Alzheimer's Disease and Type 2 Diabetes Mellitus. *CNS Neurol. Disord. Drug Targets* **2014**, *13* (7), 1280−1293.
(12) Uversky, V. N. What Does It Mean to Be Natively Unfolded? *Eur. J. Biochem.* **2002**, *269* (1), 2−12.
(13) Chiti, F.; Dobson, C. M. Amyloid Formation by Globular Proteins under Native Conditions. *Nat. Chem. Biol.* **2009**, *5* (1), 15−22.
(14) Romero, P.; Obradovic, Z.; Li, X.; Garner, E. C.; Brown, C. J.; Dunker, A. K. Sequence Complexity of Disordered Protein. *Proteins* **2001**, *42* (1), 38−48.
(15) Das, R. K.; Ruff, K. M.; Pappu, R. V. Relating Sequence Encoded Information to Form and Function of Intrinsically Disordered Proteins. *Curr. Opin Struct Biol.* **2015**, *32*, 102−112.
(16) Vugmeyster, L.; Clark, M. A.; Falconer, I. B.; Ostrovsky, D.; Gantz, D.; Qiang, W.; Hoatson, G. L. Flexibility and Solvation of Amyloid-β Hydrophobic Core. *J. Biol. Chem.* **2016**, *291* (35), 18484−18495.
(17) van Gils, J. H. M.; van Dijk, E.; Peduzzo, A.; Hofmann, A.; Vettore, N.; Schützmann, M. P.; Groth, G.; Mouhib, H.; Otzen, D. E.; Buell, A. K.; Abeln, S. The Hydrophobic Effect Characterises the Thermodynamic Signature of Amyloid Fibril Growth. *PLoS Comput. Biol.* **2020**, *16* (5), No. e1007767.
(18) Qin, M.; Wang, W.; Thirumalai, D. Protein Folding Guides Disulfide Bond Formation. *Proc. Natl. Acad. Sci. U. S. A.* **2015**, *112* (36), 11241−11246.
(19) Goers, J.; Permyakov, S. E.; Permyakov, E. A.; Uversky, V. N.; Fink, A. L. Conformational Prerequisites for Alpha-Lactalbumin Fibrillation. *Biochemistry* **2002**, *41* (41), 12546−12551, DOI: 10.1021/bi0262698.
(20) Booth, D. R.; Sunde, M.; Bellotti, V.; Robinson, C. V.; Hutchinson, W. L.; Fraser, P. E.; Hawkins, P. N.; Dobson, C. M.; Radford, S. E.; Blake, C. C.; Pepys, M. B. Instability, Unfolding and Aggregation of Human Lysozyme Variants Underlying Amyloid Fibrillogenesis. *Nature* **1997**, *385* (6619), 787−793, DOI: 10.1038/385787a0.
(21) Giugliarelli, A.; Tarpani, L.; Latterini, L.; Morresi, A.; Paolantoni, M.; Sassi, P. Spectroscopic and Microscopic Studies of Aggregation and Fibrillation of Lysozyme in Water/Ethanol Solutions. *J. Phys. Chem. B* **2015**, *119* (41), 13009−13017.
(22) Saha, S.; Sharma, A.; Deep, S. Differential Influence of Additives on the Various Stages of Insulin Aggregation. *RSC Adv.* **2016**, *6* (34), 28640−28652.
(23) Lai, Z.; Colón, W.; Kelly, J. W. The Acid-Mediated Denaturation Pathway of Transthyretin Yields a Conformational Intermediate That Can Self-Assemble into Amyloid. *Biochemistry* **1996**, *35* (20), 6470−6482.
(24) Kumar, S.; Mohanty, S. K.; Udgaonkar, J. B. Mechanism of Formation of Amyloid Protofibrils of Barstar from Soluble Oligomers: Evidence for Multiple Steps and Lateral Association Coupled to Conformational Conversion. *J. Mol. Biol.* **2007**, *367* (4), 1186−1204.
(25) Wood, S. J.; Wypych, J.; Steavenson, S.; Louis, J.-C.; Citron, M.; Biere, A. L. α-Synuclein Fibrillogenesis Is Nucleation-Dependent: IMPLICATIONS FOR THE PATHOGENESIS OF PARKINSON'S DISEASE *. *J. Biol. Chem.* **1999**, *274* (28), 19509−19512.
(26) Winner, B.; Jappelli, R.; Maji, S. K.; Desplats, P. A.; Boyer, L.; Aigner, S.; Hetzer, C.; Loher, T.; Vilar, M.; Campioni, S.; Tzitzilonis, C.; Soragni, A.; Jessberger, S.; Mira, H.; Consiglio, A.; Pham, E.; Masliah, E.; Gage, F. H.; Riek, R. In Vivo Demonstration That Alpha-Synuclein Oligomers Are Toxic. *Proc. Natl. Acad. Sci. U. S. A.* **2011**, *108* (10), 4194−4199.

(27) Karpinar, D. P.; Balija, M. B. G.; Kügler, S.; Opazo, F.; Rezaei-Ghaleh, N.; Wender, N.; Kim, H.-Y.; Taschenberger, G.; Falkenburger, B. H.; Heise, H.; Kumar, A.; Riedel, D.; Fichtner, L.; Voigt, A.; Braus, G. H.; Giller, K.; Becker, S.; Herzig, A.; Baldus, M.; Jäckle, H.; Eimer, S.; Schulz, J. B.; Griesinger, C.; Zweckstetter, M. Pre-Fibrillar α-Synuclein Variants with Impaired β-Structure Increase Neurotoxicity in Parkinson's Disease Models. *EMBO J.* **2009**, *28* (20), 3256−3268.
(28) Cecchi, C.; Stefani, M. The Amyloid-Cell Membrane System. The Interplay between the Biophysical Features of Oligomers/Fibrils and Cell Membrane Defines Amyloid Toxicity. *Biophys Chem.* **2013**, *182*, 30−43.
(29) Ahmed, M.; Davis, J.; Aucoin, D.; Sato, T.; Ahuja, S.; Aimoto, S.; Elliott, J. I.; Van Nostrand, W. E.; Smith, S. O. Structural Conversion of Neurotoxic Amyloid-β(1−42) Oligomers to Fibrils. *Nat. Struct Mol. Biol.* **2010**, *17* (5), 561−567.
(30) Quist, A.; Doudevski, I.; Lin, H.; Azimova, R.; Ng, D.; Frangione, B.; Kagan, B.; Ghiso, J.; Lal, R. Amyloid Ion Channels: A Common Structural Link for Protein-Misfolding Disease. *Proc. Natl. Acad. Sci. U. S. A.* **2005**, *102* (30), 10427−10432.
(31) Lansbury, P. T.; Lashuel, H. A. A Century-Old Debate on Protein Aggregation and Neurodegeneration Enters the Clinic. *Nature* **2006**, *443* (7113), 774−779.
(32) Bucciantini, M.; Giannoni, E.; Chiti, F.; Baroni, F.; Formigli, L.; Zurdo, J.; Taddei, N.; Ramponi, G.; Dobson, C. M.; Stefani, M. Inherent Toxicity of Aggregates Implies a Common Mechanism for Protein Misfolding Diseases. *Nature* **2002**, *416* (6880), 507−511.
(33) Ando, T.; Uchihashi, T.; Scheuring, S. Filming Biomolecular Processes by High-Speed Atomic Force Microscopy. *Chem. Rev.* **2014**, *114* (6), 3120−3188.
(34) Kim, C.; Kim, Y.; Lee, S. J.; Yun, S. R.; Choi, J.; Kim, S. O.; Yang, Y.; Ihee, H. Visualizing Heterogeneous Protein Conformations with Multi-Tilt Nanoparticle-Aided Cryo-Electron Microscopy Sampling. *Nano Lett.* **2023**, *23* (8), 3334−3343.
(35) Karamanos, T. K.; Kalverda, A. P.; Thompson, G. S.; Radford, S. E. Mechanisms of Amyloid Formation Revealed by Solution NMR. *Prog. Nucl. Magn. Reson. Spectrosc.* **2015**, *0*, 86−104.
(36) Hou, L.; Shao, H.; Zhang, Y.; Li, H.; Menon, N. K.; Neuhaus, E. B.; Brewer, J. M.; Byeon, I.-J. L.; Ray, D. G.; Vitek, M. P.; Iwashita, T.; Makula, R. A.; Przybyla, A. B.; Zagorski, M. G. Solution NMR Studies of the Aβ(1−40) and Aβ(1−42) Peptides Establish That the Met35 Oxidation State Affects the Mechanism of Amyloid Formation. *J. Am. Chem. Soc.* **2004**, *126* (7), 1992−2005.
(37) Tycko, R. Solid-State NMR Studies of Amyloid Fibril Structure. *Annu. Rev. Phys. Chem.* **2011**, *62* (1), 279−299.
(38) Li, Y.; Zhao, C.; Luo, F.; Liu, Z.; Gui, X.; Luo, Z.; Zhang, X.; Li, D.; Liu, C.; Li, X. Amyloid Fibril Structure of α-Synuclein Determined by Cryo-Electron Microscopy. *Cell Res.* **2018**, *28* (9), 897−903.
(39) Ratha, B. N.; Kar, R. K.; Brender, J. R.; Pariary, R.; Sahoo, B.; Kalita, S.; Bhunia, A. High-Resolution Structure of a Partially Folded Insulin Aggregation Intermediate. *Proteins: Struct., Funct., Bioinf.* **2020**, *88* (12), 1648−1659.
(40) Lawrence, M. C. Understanding Insulin and Its Receptor from Their Three-Dimensional Structures. *Mol. Metab* **2021**, *52*, No. 101255.
(41) Whittingham, J. L.; Scott, D. J.; Chance, K.; Wilson, A.; Finch, J.; Brange, J.; Guy Dodson, G. Insulin at pH 2: Structural Analysis of the Conditions Promoting Insulin Fibre Formation. *J. Mol. Biol.* **2002**, *318* (2), 479−490.
(42) Hua, Q.-X.; Jia, W.; Frank, B. H.; Phillips, N. F. B.; Weiss, M. A. A Protein Caught in a Kinetic Trap: Structures and Stabilities of Insulin Disulfide Isomers. *Biochemistry* **2002**, *41* (50), 14700−14715.
(43) van Lierop, B.; Ong, S. C.; Belgi, A.; Delaine, C.; Andrikopoulos, S.; Haworth, N. L.; Menting, J. G.; Lawrence, M. C.; Robinson, A. J.; Forbes, B. E. Insulin in Motion: The A6-A11 Disulfide Bond Allosterically Modulates Structural Transitions Required for Insulin Activity. *Sci. Rep* **2017**, *7* (1), 17239.
(44) Mayer, J. P.; Zhang, F.; DiMarchi, R. D. Insulin Structure and Function. *Peptide Science* **2007**, *88* (5), 687−713.
(45) Dodson, G.; Steiner, D. The Role of Assembly in Insulin's Biosynthesis. *Curr. Opin. Struct. Biol.* **1998**, *8* (2), 189−194.
(46) Brange, J.; Andersen, L.; Laursen, E. D.; Meyn, G.; Rasmussen, E. Toward Understanding Insulin Fibrillation. *J. Pharm. Sci.* **1997**, *86* (5), 517−525.
(47) Hefford, M. A.; Oda, G.; Kaplan, H. Structure-Function Relationships in the Free Insulin Monomer. *Biochem. J.* **1986**, *237* (3), 663−668.
(48) Nielsen, L.; Khurana, R.; Coats, A.; Frokjaer, S.; Brange, J.; Vyas, S.; Uversky, V. N.; Fink, A. L. Effect of Environmental Factors on the Kinetics of Insulin Fibril Formation: Elucidation of the Molecular Mechanism. *Biochemistry* **2001**, *40* (20), 6036−6046.
(49) Dische, F. E.; Wernstedt, C.; Westermark, G. T.; Westermark, P.; Pepys, M. B.; Rennie, J. A.; Gilbey, S. G.; Watkins, P. J. Insulin as an Amyloid-Fibril Protein at Sites of Repeated Insulin Injections in a Diabetic Patient. *Diabetologia* **1988**, *31* (3), 158−161.
(50) D'Souza, A.; Theis, J. D.; Vrana, J. A.; Dogan, A. Pharmaceutical Amyloidosis Associated with Subcutaneous Insulin and Enfuvirtide Administration. *Amyloid* **2014**, *21* (2), 71−75.
(51) Ahmad, A.; Millett, I. S.; Doniach, S.; Uversky, V. N.; Fink, A. L. Partially Folded Intermediates in Insulin Fibrillation. *Biochemistry* **2003**, *42* (39), 11404−11416.
(52) Zako, T.; Sakono, M.; Hashimoto, N.; Ihara, M.; Maeda, M. Bovine Insulin Filaments Induced by Reducing Disulfide Bonds Show a Different Morphology, Secondary Structure, and Cell Toxicity from Intact Insulin Amyloid Fibrils. *Biophys. J.* **2009**, *96* (8), 3331−3340.
(53) Chatani, E.; Imamura, H.; Yamamoto, N.; Kato, M. Stepwise Organization of the β-Structure Identifies Key Regions Essential for the Propagation and Cytotoxicity of Insulin Amyloid Fibrils. *J. Biol. Chem.* **2014**, *289* (15), 10399−10410.
(54) Ivanova, M. I.; Sievers, S. A.; Sawaya, M. R.; Wall, J. S.; Eisenberg, D. Molecular Basis for Insulin Fibril Assembly. *Proc. Natl. Acad. Sci. U. S. A.* **2009**, *106* (45), 18990−18995.
(55) Nayak, A.; Sorci, M.; Krueger, S.; Belfort, G. A Universal Pathway for Amyloid Nucleus and Precursor Formation for Insulin. *Proteins* **2009**, *74* (3), 556−565.
(56) Ahmad, A.; Uversky, V. N.; Hong, D.; Fink, A. L. Early Events in the Fibrillation of Monomeric Insulin. *J. Biol. Chem.* **2005**, *280* (52), 42669−42675.
(57) Nielsen, L.; Frokjaer, S.; Carpenter, J. F.; Brange, J. Studies of the Structure of Insulin Fibrils by Fourier Transform Infrared (FTIR) Spectroscopy and Electron Microscopy. *J. Pharm. Sci.* **2001**, *90* (1), 29−37.
(58) Bouchard, M.; Zurdo, J.; Nettleton, E. J.; Dobson, C. M.; Robinson, C. V. Formation of Insulin Amyloid Fibrils Followed by FTIR Simultaneously with CD and Electron Microscopy. *Protein Sci.* **2000**, *9* (10), 1960−1967.
(59) Greenfield, N. J. Using Circular Dichroism Spectra to Estimate Protein Secondary Structure. *Nat. Protoc* **2006**, *1* (6), 2876−2890.
(60) Maiti, N. C.; Apetri, M. M.; Zagorski, M. G.; Carey, P. R.; Anderson, V. E. Raman Spectroscopic Characterization of Secondary Structure in Natively Unfolded Proteins: α-Synuclein. *J. Am. Chem. Soc.* **2004**, *126* (8), 2399−2408.
(61) Apetri, M. M.; Maiti, N. C.; Zagorski, M. G.; Carey, P. R.; Anderson, V. E. Secondary Structure of α-Synuclein Oligomers: Characterization by Raman and Atomic Force Microscopy. *J. Mol. Biol.* **2006**, *355* (1), 63−71.
(62) Dolui, S.; Mondal, A.; Roy, A.; Pal, U.; Das, S.; Saha, A.; Maiti, N. C. Order, Disorder, and Reorder State of Lysozyme: Aggregation Mechanism by Raman Spectroscopy. *J. Phys. Chem. B* **2020**, *124* (1), 50−60.
(63) Dolui, S.; Roy, A.; Pal, U.; Saha, A.; Maiti, N. C. Structural Insight of Amyloidogenic Intermediates of Human Insulin. *ACS Omega* **2018**, *3* (2), 2452−2462.
(64) Filik, J.; Stone, N. Drop Coating Deposition Raman Spectroscopy of Protein Mixtures. *Analyst* **2007**, *132* (6), 544−550.
(65) Roy, A.; Chandra, K.; Dolui, S.; Maiti, N. C. Envisaging the Structural Elevation in the Early Event of Oligomerization of Disordered Amyloid β Peptide. *ACS Omega* **2017**, *2* (8), 4316−4327.

https://doi.org/10.1021/acsphyschemau.3c00065
ACS Phys. Chem Au 2024, 4, 268−280

(66) Huang, K.; Maiti, N. C.; Phillips, N. B.; Carey, P. R.; Weiss, M. A. Structure-Specific Effects of Protein Topology on Cross-β Assembly: Studies of Insulin Fibrillation. *Biochemistry* **2006**, *45* (34), 10278−10293.
(67) Mikhonin, A. V.; Ahmed, Z.; Ianoul, A.; Asher, S. A. Assignments and Conformational Dependencies of the Amide III Peptide Backbone UV Resonance Raman Bands. *J. Phys. Chem. B* **2004**, *108* (49), 19020−19028.
(68) Dong, J.; Wan, Z.; Popov, M.; Carey, P. R.; Weiss, M. A. Insulin Assembly Damps Conformational Fluctuations: Raman Analysis of Amide I Linewidths in Native States and Fibrils. *J. Mol. Biol.* **2003**, *330* (2), 431−442.
(69) Zheng, R.; Zheng, X.; Dong, J.; Carey, P. R. Proteins Can Convert to β-Sheet in Single Crystals. *Protein Sci.* **2004**, *13* (5), 1288−1294.
(70) Tuma, R. Raman Spectroscopy of Proteins: From Peptides to Large Assemblies. *J. Raman Spectrosc.* **2005**, *36* (4), 307−319.
(71) Zeng, G.; Shou, J.-J.; Li, K.-K.; Zhang, Y.-H. In-Situ Confocal Raman Observation of Structural Changes of Insulin Crystals in Sequential Dehydration Process. *Biochim. Biophys. Acta* **2011**, *1814* (12), 1631−1640.
(72) Sereda, V.; Sawaya, M. R.; Lednev, I. K. Structural Organization of Insulin Fibrils Based on Polarized Raman Spectroscopy: Evaluation of Existing Models. *J. Am. Chem. Soc.* **2015**, *137* (35), 11312−11320.
(73) Ramya, A. N.; Joseph, M. M.; Nair, J. B.; Karunakaran, V.; Narayanan, N.; Maiti, K. K. New Insight of Tetraphenylethylene-Based Raman Signatures for Targeted SERS Nanoprobe Construction Toward Prostate Cancer Cell Detection. *ACS Appl. Mater. Interfaces* **2016**, *8* (16), 10220−10225.
(74) Murali, V. P.; Karunakaran, V.; Murali, M.; Lekshmi, A.; Kottarathil, S.; Deepika, S.; Saritha, V. N.; Ramya, A. N.; Raghu, K. G.; Sujathan, K.; Maiti, K. K. A Clinically Feasible Diagnostic Spectro-Histology Built on SERS-Nanotags for Multiplex Detection and Grading of Breast Cancer Biomarkers. *Biosens. Bioelectron.* **2023**, *227*, No. 115177.
(75) Karunakaran, V.; Saritha, V. N.; Joseph, M. M.; Nair, J. B.; Saranya, G.; Raghu, K. G.; Sujathan, K.; Kumar, K. S.; Maiti, K. K. Diagnostic Spectro-Cytology Revealing Differential Recognition of Cervical Cancer Lesions by Label-Free Surface Enhanced Raman Fingerprints and Chemometrics. *Nanomedicine* **2020**, *29*, No. 102276.
(76) Joseph, M. M.; Narayanan, N.; Nair, J. B.; Karunakaran, V.; Ramya, A. N.; Sujai, P. T.; Saranya, G.; Arya, J. S.; Vijayan, V. M.; Maiti, K. K. Exploring the Margins of SERS in Practical Domain: An Emerging Diagnostic Modality for Modern Biomedical Applications. *Biomaterials* **2018**, *181*, 140−181.
(77) Rygula, A.; Majzner, K.; Marzec, K. M.; Kaczor, A.; Pilarczyk, M.; Baranska, M. Raman Spectroscopy of Proteins: A Review. *J. Raman Spectrosc.* **2013**, *44* (8), 1061−1076.
(78) Wen, Z.-Q. Raman Spectroscopy of Protein Pharmaceuticals. *J. Pharm. Sci.* **2007**, *96* (11), 2861−2878.
(79) Kocherbitov, V.; Latynis, J.; Misiūnas, A.; Barauskas, J.; Niaura, G. Hydration of Lysozyme Studied by Raman Spectroscopy. *J. Phys. Chem. B* **2013**, *117* (17), 4981−4992.
(80) Tsuboi, M.; Suzuki, M.; Overman, S. A.; Thomas, G. J. Intensity of the Polarized Raman Band at 1340−1345 Cm-1 As an Indicator of Protein α-Helix Orientation: Application to Pf1 Filamentous Virus. *Biochemistry* **2000**, *39* (10), 2677−2684.
(81) Barik, S. The Uniqueness of Tryptophan in Biology: Properties, Metabolism, Interactions and Localization in Proteins. *Int. J. Mol. Sci.* **2020**, *21* (22), 8776.
(82) Pace, C. N.; Horn, G.; Hebert, E. J.; Bechert, J.; Shaw, K.; Urbanikova, L.; Scholtz, J. M.; Sevcik, J. Tyrosine Hydrogen Bonds Make a Large Contribution to Protein stability11Edited by C. R. Matthews. *J. Mol. Biol.* **2001**, *312* (2), 393−404.
(83) Bekard, I. B.; Dunstan, D. E. Tyrosine Autofluorescence as a Measure of Bovine Insulin Fibrillation. *Biophys. J.* **2009**, *97* (9), 2521−2531.
(84) Shi, L.; Li, Y.; Li, Z. Early Cancer Detection by SERS Spectroscopy and Machine Learning. *Light Sci. Appl.* **2023**, *12* (1), 234.
(85) Dong, S.; Wang, Y.; Liu, Z.; Zhang, W.; Yi, K.; Zhang, X.; Zhang, X.; Jiang, C.; Yang, S.; Wang, F.; Xiao, X. Beehive-Inspired Macroporous SERS Probe for Cancer Detection through Capturing and Analyzing Exosomes in Plasma. *ACS Appl. Mater. Interfaces* **2020**, *12* (4), 5136−5146.
(86) Yang, Y.; Petkova, A.; Huang, K.; Xu, B.; Hua, Q.-X.; Ye, I.-J.; Chu, Y.-C.; Hu, S.-Q.; Phillips, N. B.; Whittaker, J.; Ismail-Beigi, F.; Mackin, R. B.; Katsoyannis, P. G.; Tycko, R.; Weiss, M. A. An Achilles' Heel in an Amyloidogenic Protein and Its Repair: Insulin Fibrillation and Therapeutic Design. *J. Biol. Chem.* **2010**, *285* (14), 10806−10821.
(87) Thornton, J. M. Disulphide Bridges in Globular Proteins. *J. Mol. Biol.* **1981**, *151* (2), 261−287.
(88) Hogg, P. J. Disulfide Bonds as Switches for Protein Function. *Trends Biochem. Sci.* **2003**, *28* (4), 210−214.
(89) Kurouski, D.; Washington, J.; Ozbil, M.; Prabhakar, R.; Shekhtman, A.; Lednev, I. K. Disulfide Bridges Remain Intact While Native Insulin Converts into Amyloid Fibrils. *PLoS One* **2012**, *7* (6), No. e36989.
(90) Kitagawa, T.; Hirota, S. Raman Spectroscopy of Proteins. In *Handbook of Vibrational Spectroscopy*; John Wiley & Sons, Ltd, 2006.
(91) Vestergaard, B.; Groenning, M.; Roessle, M.; Kastrup, J. S.; de Weert, M. v.; Flink, J. M.; Frokjaer, S.; Gajhede, M.; Svergun, D. I.; Bjorkman, P. J. A Helical Structural Nucleus Is the Primary Elongating Unit of Insulin Amyloid Fibrils. *PLoS Biol.* **2007**, *5* (5), No. e134.
(92) Hayden, E. Y.; Teplow, D. B. Amyloid β-Protein Oligomers and Alzheimer's Disease. *Alzheimers Res. Ther* **2013**, *5* (6), 60.

https://doi.org/10.1021/acsphyschemau.3c00065
ACS Phys. Chem Au 2024, 4, 268−280